Inorg. Chem. **2005**, *44*, 8349–8354

Sulfur K-Edge XAS and DFT Calculations on $[Fe_4S_4]^{2+}$ Clusters: Effects of H-bonding and Structural Distortion on Covalency and Spin Topology

Abhishek Dey,[†] Cara L. Roche,[§] Marc A. Walters,*[,§] Keith O. Hodgson,*[,†,‡] Britt Hedman,*[,‡] and Edward I. Solomon*[,†]

Department of Chemistry, Stanford University, Stanford, California 94305, Stanford Synchrotron Radiation Laboratory, SLAC, Menlo Park, California 94302, and Department of Chemistry, New York University, New York 10003

Received June 15, 2005

Sulfur K-edge X-ray absorption spectroscopy of a hydrogen-bonded elongated $[Fe_4S_4]^{2+}$ cube is reported. The data show that this synthetic cube is less covalent than a normal compressed cube with no hydrogen bonding. DFT calculations reveal that the observed difference in electronic structure has significant contributions from both the cluster distortion and from hydrogen bonding. The elongated and compressed Fe_4S_4 structures are found to have different spin topologies (i.e., orientation of the delocalized Fe_2S_2 subclusters which are antiferromagnetically coupled to each other). It is suggested that the H-bonding interaction with the counterion does not contribute to the cluster elongation. A magneto-structural correlation is developed for the Fe_4S_4 cube that is used to identify the redox-active Fe_2S_2 subclusters in active sites of HiPIP and ferredoxin proteins involving these clusters.

Introduction

Iron−sulfur active sites perform a broad variety of functions in biological systems ranging from electron transfer (ET) to small molecule activation. In the ET proteins, they exist as mononuclear (rubredoxins), binuclear (plant ferredoxins), trinuclear (ferredoxins II), and tetranuclear (bacterial ferredoxins and High Potential Proteins) Fe−S clusters.[1−3] Their $E°$ values span the physiological range from −700 to +600 mV. They have low reorganization energies which make them ideal for ET.

The unique electronic structures of these clusters have been studied extensively using a number of experimental and computational methods.[4] Electronic spectroscopy of these active sites is solely dominated by intense S → Fe charge-transfer transitions which indicate high covalency for the Fe−S bonds. Mössbauer spectroscopy has indicated that while the mixed-valence binuclear Fe_2S_2 sites are localized, the trinuclear and the tetranuclear sites are delocalized.[3] It has been found that the interplay among metal−metal double-exchange (β),[5] ligand super-exchange (J),[6] vibronic coupling, and spin frustration[7] determines the extent of delocalization.[8]

The redox potentials of the protein active sites are generally found to be ∼500−1000 mV more positive than those of the related model complexes. The factors contributing to such dramatic shifts in redox potentials are the subject of active research. Hydrogen bonding from the backbone to the cluster ligands and dipoles around the clusters, as well as local dielectric environment in the protein are thought to be major contributors to this observed increase in redox potential. The H-bonding interaction is thought to be involved in ET pathways.

Significant research effort has been devoted toward understanding and modeling these effects using synthetic, spectroscopic, and computational chemistry.[9−12] Sulfur K-

* To whom correspondence should be addressed. E-mail: Edward.solomon@stanford.edu (E.I.S.); marc.walters@nyu.edu (M.C.A.); Hedman@ssrl.slac.stanford.edu (B.H.); Hodgson@ssrl.slac.stanford.edu (K.O.H.).

† Stanford University.

‡ Stanford Synchrotron Radiation Laboratory.

§ New York University.

(1) Fukuyama, K. *Photosynth. Res.* **2004**, *81*, 289−301.
(2) Beinert, H. *J. Biol. Inorg. Chem* **2000,** *5*, 2−15.
(3) Beinert, H., Holm, R. H.; Münck, E. *Science* **1997**, *277*, 653−659.
(4) Noodleman, L.; Peng, C. Y.; Case, D. A.; Mouesca, J. M. *Coord. Chem. Rev.* **1995**, *144*, 199−244.
(5) Girerd, J.-J. *J. Chem. Phys.* **1983**, *79*, 1766.
(6) Kramer, A. *Physica* **1934**, *1*, 191.
(7) Toulouse, G. *Comm. Phys. (London)* **1977**, *2*, 115.
(8) Glaser, T.; Rose, K. W.; Shadle, S. E.; Hedman, B.; Hodgson, K. O.; Solomon, E. I. *J. Am. Chem. Soc.* **2001**, *123*, 442−454.
(9) Park, I. Y.; Youn, B.; Harley, J. L.; Eidsness, M. K.; Smith, E.; Ichiye, T.; Kang, C. H. *J. Biol. Inorg. Chem.* **2004**, *9*, 423−428.
(10) Ueyama, N.; Yamada, Y.; Okamura, T.; Kimura, S.; Nakamura, A. *Inorg. Chem.* **1996**, *22*, 6473−6484.
(11) Yang, X.; Niu, S. Q.; Ichiye, T.; Wang, L. S. *J. Am. Chem. Soc.* **2004**, *126*, 15790−15794.
(12) Torres, R. A.; Lovell, T.; Noodleman, L.; Case, D. A. *J. Am. Chem. Soc.* **2003**, *125*, 1923−1936.

10.1021/ic050981m CCC: $30.25
Published on Web 10/08/2005

Scheme 1. (**1**) Compressed Non-H-Bonded Cluster (**2**) Elongated H-bonded Cluster (N···S distances shown in red)

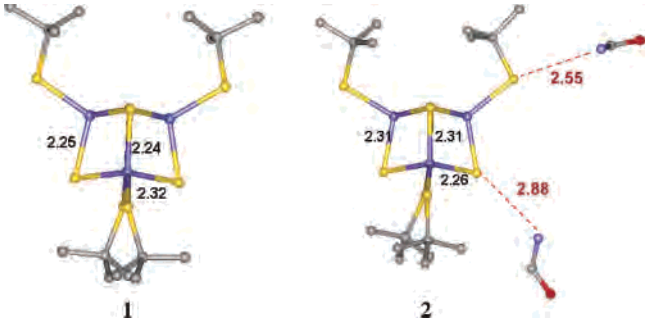

edge X-ray absorbtion spectroscopy (XAS) has been developed to directly probe the covalency of the Fe−S bonds and has also been found to be sensitive to the effects of the H-bonding interactions on the electronic structures of these active sites.[13] This technique probes the transitions from the 1s orbitals of the sulfur ligands (thiolates, sulfides) to the singly or unoccupied metal 3d orbitals ($1s \rightarrow \psi^*$, where $\psi^* = (1 - \alpha^2)^{1/2} |3d> + \alpha|S_{3p}>$). This transition is allowed due to the S 3p mixing into the metal 3d orbitals due to covalency.[14] Hence, the observed intensity quantitates the covalency of the Fe−S bond and the effect of the ligand environment on this.

It has been found, using this technique, that the Fe−S bond covalency is significantly reduced in the mononuclear, binuclear, trinuclear, and tetranuclear protein active sites relative to their corresponding model complexes.[15−17] It has also been found using S K-edge XAS that the reduction in covalency correlates with the observed increase in reduction potential. Recently, this has been quantitatively studied in a series of thiolate heme model complexes where the redox potential has been found to vary approximately linearly with Fe−S bond covalency.[18] Walters et al. reported the synthesis of the complex $[CTA]_4[Fe_4S_4(S\text{-}t\text{-}Bu)_4]$ (**2**) which has two H-bonding interactions (one with a $\mu_3S_{sulfide}$ and one with a $S_{thiolate}$).[19] This cluster also has an elongated core, which is unusual for this oxidation state. In the present study, we investigate the electronic structure of the iron−sulfur cube in this cluster in its $[Fe_4S_4]^{2+}$ oxidation state using S K-edge XAS and DFT calculations and compare this electronic structure to that of the Fe_4S_4 cube in $[NEt_4]_2[Fe_4S_4(S\text{-}t\text{-}Bu)_4]$ (**1**) (Scheme 1), which has no hydrogen bonding and is the more generally observed compressed cube core structure.

Experimental and Computational Details

The complexes $[NEt_4]_2[Fe_4S_4(S\text{-}t\text{-}Bu)_4]$ (**1**) and $[CTA]_4[Fe_4S_4(S\text{-}t\text{-}Bu)_4]$ (**2**) were prepared as described elsewhere.[19] For XAS experiments, sample preparations were performed in a dry, nitrogen-filled, anaerobic-atmosphere glovebox. The samples were ground into a fine powder and dispersed as thinly as possible on sulfur-free Mylar tape. This procedure has been verified to minimize self-absorption effects. The samples were then mounted across the window of an aluminum plate. A 6.35 μm polypropylene film window protected the solid samples from exposure to air during transfer from the glovebox to the experimental sample chamber. XAS data were measured at the Stanford Synchrotron Radiation Laboratory using the 54-pole wiggler beam line 6−2 at 3 GeV/80−100 mA ring conditions. Details of the experimental configuration for low-energy studies and data reduction methods have been described.[20]

Pre-edge features were fit using pseudo-Voigt line shapes (sums of Lorentzian and Gaussian functions). This line shape is appropriate, as the experimental features are expected to be a convolution of a Lorentzian transition envelope and a Gaussian line shape imposed by the beam-line spectrometer optics.[21,22] A fixed 1:1 ratio of Lorentzian to Gaussian contributions successfully reproduced the pre-edge features. The rising edge functions were also fit with pseudo-Voigt line shapes. Good fits reproduce the data using a minimum number of peaks. In contrast to our studies on other Fe_4S_4 clusters, the $\mu_3S_{sulfide}$ and the $S_{thiolate}$ contributions could not be resolved in the data due to comparable Z_{eff} (effective nuclear charge of the S atom) of $\mu_3S_{sulfide}$ and $S_{thiolate}$ (vide-infra). Therefore, only the total integrated intensity was used for comparison to DFT calculations.

All calculations were performed on dual-CPU Pentium Xeon 2.8 GHz workstations using the Amsterdam Density Functional (ADF) program, version 2004.01, developed by Baerends et al.[23,24] A triple-ζ Slater-type orbital basis set (ADF basis set TZP) with a single polarization function at the local density approximation of Vosko, Wilk, and Nusair[25] with nonlocal gradient corrections of Becke[26] and Perdew[27] were employed. The Mulliken population analyses[28] were performed using the output file of ADF program. Broken symmetry[29] calculation was implemented (for both single points and geometry optimizations) by using the MODIFYSTART-POTENTIAL keyword where an initial spin-polarization is imposed which is then allowed to relax to obtain the converged ground state. The stability of the converged wave functions were tested by increasing the basis set, changing the functional, and by starting with different spin-polarizations (M_S) for the $[Fe_2S_2]^+$ subclusters, all of which resulted in equivalent descriptions of the ground state. For DFT calculations, the *tert*-butyl groups were simplified to methyl groups for both the single-point and geometry-optimized calculations. Likewise, the H-bonded counterion was truncated to a formamide group.

(13) Solomon, E. I.; Hedman, B.; Hodgson, K. O.; Dey, A.; Szilagyi, R. K. *Coord. Chem. Rev.* **2005**, *249*, 97−129.
(14) Neese, F.; Hedman, B.; Hodgson, K. O.; Solomon, E. I. *Inorg. Chem.* **1999**, *38*, 4854−4860.
(15) Anxolabéhère-Mallart, E.; Glaser, T.; Frank, P.; Aliverti, A.; Zanetti, G.; Hedman, B.; Hodgson, K. O.; Solomon, E. I. *J. Am. Chem. Soc.* **2001**, *123*, 5444−5452.
(16) Dey, A.; Glaser, T.; Moura, J. J. G.; Holm, R. H.; Hedman, B.; Hodgson, K. O.; Solomon, E. I. *J. Am. Chem. Soc.* **2004**, *126*, 16868−16878.
(17) Glaser, T.; Bertini, I.; Moura, J. J. G.; Hedman, B.; Hodgson, K. O.; Solomon, E. I. *J. Am. Chem. Soc.* **2001**, *123*, 4859−4860.
(18) Dey, A.; Okamura, T.; Ueyama, N.; Hedman, B.; Hodgson, K. O.; Solomon, E. I. *J. Am. Chem. Soc.* **2005**, *127*, 12046−12053.
(19) Walters, M. A.; Roche, C. L.; Rheingold, A. L.; Kassel, S. W. *Inorg. Chem.* **2005**, *44*, 3777−3779.
(20) Hedman, B.; Frank, P.; Gheller, S. F.; Roe, A. L.; Newton, W. E.; Hodgson, K. O. *J. Am. Chem. Soc.* **1988**, *110*, 3798−3805.
(21) Agarwal, B. K. *X-ray Spectroscopy*; Springer-Verlag: Berlin, 1979; p 276.
(22) Tyson, T. A.; Roe, A. L.; Frank, P.; Hodgson, K. O.; Hedman, B. *Phys. Rev. B* **1989**, *39A*, 6305−6315.
(23) Baerends, E. J.; Ellis, D. E.; Ros, P. *Chem. Phys.* **1973**, *2*, 41−51.
(24) te Velde, G.; Baerends, E. J. *Int. J. Comput. Phys.* **1992**, *99*, 84−98.
(25) Vosko, S. H.; Wilk, L.; Nusair, M. *Can. J. Phys.* **1980**, *58*, 1200−1211.
(26) Becke, A. D. *Phys. Rev. A: Gen. Phys.* **1988**, *38*, 3098−3100.
(27) Perdew, J. P. *Phys. Rev. B* **1986**, *33*, 8822−8824.
(28) Mulliken, R. S. *J. Chem. Phys.* **1955**, *23*, 1833−1840.
(29) Noodleman, L.; Baerends, E. J. *J. Am. Chem. Soc.* **1984**, *106*, 2316−2327.

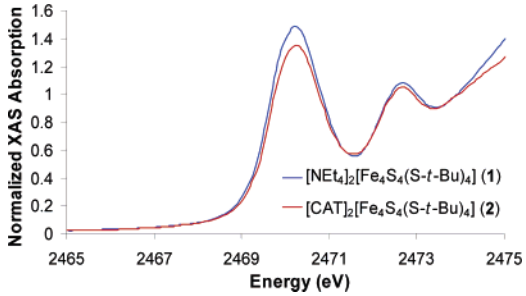

Figure 1. S K-edge XAS of complexes **1** (blue) and **2** (red).

Results and Analysis

The S K-edge XAS data for both the $[NEt_4]_2[Fe_4S_4(S\text{-}t\text{-butyl})_4]$ and $[CTA]_2[Fe_4S_4(S\text{-}t\text{-butyl})_4]$ complexes (Figure 1) show an envelope of transitions from 1s orbitals of sulfide and thiolate to the singly occupied Fe_{3d} orbitals in the range of 2469−2471 eV (pre-edge; maximum at 2470.3 eV), and a higher-energy transition from the 1s orbitals to C−S σ^* orbitals of the thiolates at 2473 eV. Both transitions gain intensity due to covalent mixing of S_{3p} character into the acceptor orbitals. The intensity of the pre-edge for the H-bonded complex (**2**) is less than that of complex **1**, while there is no change in energy position of the pre-edge.

The pre-edge peak intensities obtained by fitting the data were 2.52 for **1** and 2.32 for **2** (Figure 1). Note that the second derivatives of the data (where a minimum represents the presence of a peak maximum) do not require the presence of two resolvable transitions, from the $\mu_3S_{sulfide}$ and the $S_{thiolate}$, as observed for $[Fe_4S_4(SPh)_4]^{2-}$ (lack of two features in the second derivative of **1** compared to $[Fe_4S_4(SPh)_4]^{2-}$ in Figure S1; Supporting Information). This is due to the stronger electron-donating effect of the bulkier *tert*-butyl group relative to the electron-withdrawing effect of a phenyl group, which shifts the 1s orbitals of the *tert*-butyl $S_{thiolate}$ to higher energy, hence shifting it closer to that of the $\mu_3S_{sulfide}$. This leads to overlap of the pre-edge transition of the $S_{thiolate}$ with that of the $\mu_3S_{sulfide}$. The total decrease in intensity (i.e., covalency) can, however, be quantified as 0.2 (difference between 2.52 in **1** and 2.32 in **2**) units of total normalized intensity. Conversion to a change in covalency requires knowledge of the relative contributions of the $S_{thiolate}$ and the $S_{sulfide}$, which could not be resolved experimentally. However, an estimate of this ratio can be obtained from DFT calculations.

The experimentally observed change in electronic structure of complex **2** relative to that of **1** can have contributions from two factors. First, the H-bonding interaction with the donor ligands will reduce Fe−S bond covalency in **2**. This involves a $\mu_3S_{sulfide}$ with H−N of the amide nitrogen of the counterion and a $S_{thiolate}$ with H−N of an amide nitrogen from a second counterion (Scheme 1). Second, the change in geometric structure of **2** relative to that of **1** can also affect covalency. The relative contribution of these effects was estimated using DFT calculations performed on a simplified model $[Fe_4S_4(SMe)_4]^{2-}$ where the cluster geometries (obtained crystallographically) were kept intact, but the bulky *tert*-butyl groups were modeled by methyl groups and the H-bonding interactions with the counterions were modeled with formamide.[30]

The electronic structure of **1**, calculated using Broken symmetry DFT calculations, shows that the $S = 0$ $[Fe_4S_4]^{2+}$ cube has two valence-delocalized, high-spin ($S = 9/2$), $[Fe_2S_2]^+$ subclusters (color coded blue and red in Scheme 2) which are antiferromagnetically coupled to each other, in agreement with previous experimental and computational results.[3,4,8] The total covalency of **1** (total % S_{3p} character summed over the 18 (9α or 9β) Fe_{3d} holes) for 4 $\mu_3S_{sulfide}$ and 4 $S_{thiolate}$ of an Fe_2S_2 subcluster is 296% and 102%, respectively. These estimates are in good agreement with previous calculations reported for $[Fe_4S_4]^{2+}$ cubes.[31] The calculated covalencies for **2** having same spin topology as **1** are 284% and 82% for $\mu_3S_{sulfide}$ and $S_{thiolate}$, respectively. The $\mu_3S_{sulfide}$ covalency decreases by 12% and the $S_{thiolate}$ covalency decreases by 20% from **1** to **2**, which would be consistent with the stronger hydrogen-bonding interaction of the counterion with the $S_{thiolate}$ (N···S = 2.55 Å) in **2**. Since the individual Fe−S bond covalencies could not be resolved from the data for **1** and **2**, the calculated Fe−S bond covalencies were scaled by their respective transition moments (6.54 for $\mu_3S_{sulfide}$ and 8.15 for $S_{thiolate}$) to estimate the total calculated pre-edge intensity change that can be correlated to the data. The calculated XAS pre-edge intensity of **1** is 1.47 units compared to the 2.52 units obtained experimentally. An underestimate of Fe−S bonding at the GGA level of DFT calculations has been reported previously.[31]

Complex **2** has two H-bonding interactions and is elongated along the C_2 axis of symmetry. Scheme 2 presents a decomposition of the calculated decrease of Fe−S bond covalency in **2** relative to **1** into its individual contributions from the structural distortion and the H-bonding interactions. The top structure represents the starting molecule (**1**) which is non-H-bonded and compressed along the C_2 axis (the C_2 axis is normal to the center of the two delocalized Fe_2S_2 subclusters colored in blue and red). The numbers below the cluster and in Table 1 represent the calculated $\mu_3S_{sulfide}$, $S_{thiolate}$, and total intensity, respectively. On elongation of the cluster (Scheme 2, left and Table 1, row 2), the calculated Fe−$S_{thiolate}$ covalency decreases by 0.08 units due to the shortening of the two Fe−$S_{sulfide}$ bonds in the subcluster, which weakens the Fe−$S_{thiolate}$ covalency, as sulfide is a stronger donor. Introduction of H-bonding to this elongated cluster results in a further decrease in the intensity (for both sulfide and thiolate, Table 1, row 4) from 1.47 in **1** to 1.34 in **2**, i.e., a total change of 0.13 units, which is in reasonable agreement with the rescaled experimental data (0.11 units).[32] Alternatively, introducing two H-bonding interactions on the

(30) Note that DFT calculations of the ground state of a $[Fe_4S_4]^{2+}$ cube with −S-*t*-Bu and −SMe show that the thiolate covalency is almost identical (49% vs 51%) for fixed Fe−$S_{thiolate}$ bond length.

(31) Dey, A.; Glaser, T.; Couture, M. M. J.; Eltis, L. D.; Holm, R. H.; Hedman, B.; Hodgson, K. O.; Solomon, E. I. *J. Am. Chem. Soc.* **2004**, *126*, 8320−8328.

(32) The observed intensity change of 0.20 units in the XAS spectra has to be rescaled by a factor of 1.7 (observed intensity for **1**/calculated intensity for **1**, i.e., 2.52/1.47 = 1.7) to 0.11 for comparison to the calculated changes.

Scheme 2. Decomposition of the Total Change in Bonding into Structural and H-bonding Components[a]

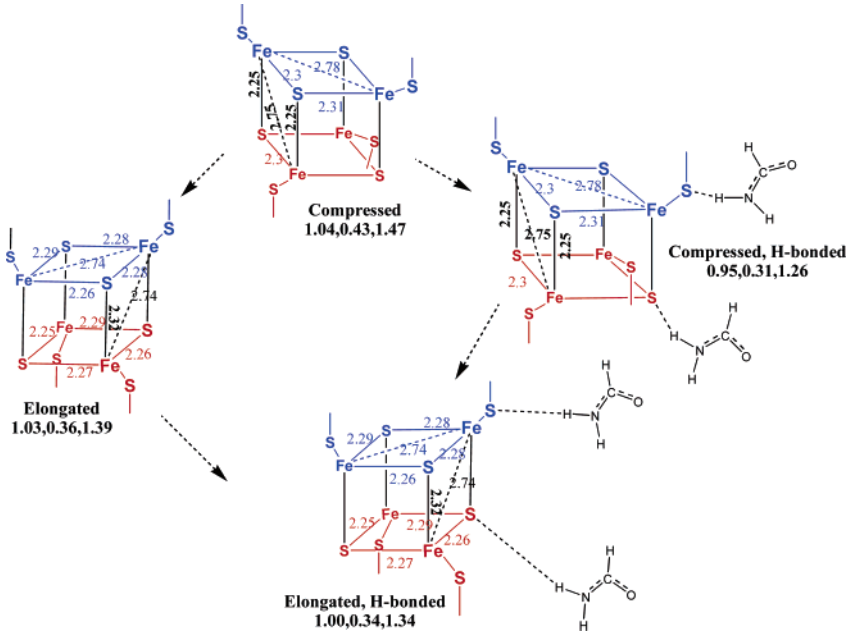

[a] The calculated intensities are listed next to the structures ($\mu_3S_{sulfide}$, $S_{thiolate}$, and total, respectively). The two delocalized $[Fe_2S_2]^+$ subclusters are color-coded blue and red. The bridging Fe−S bonds are colored black. Compressed and elongated implies that these bridging Fe−S bonds (in black) are shorter and longer, respectively.

Table 1. Calculated Ligand Covalencies for Scheme 2

core structure	$\mu_3S_{sulfide}$	$S_{thiolate}$	total
$[Fe_4S_4]^{2+}$ compressed	1.04	0.43	1.47
$[Fe_4S_4]^{2+}$ elongated	1.03	0.36	1.39
$[Fe_4S_4]^{2+}$ compressed H-bonded	0.95	0.31	1.26
$[Fe_4S_4]^{2+}$ elongated H-bonded (vertical)	1.00	0.34	1.34
$[Fe_4S_4]^{2+}$ elongated H-bonded (horizontal)	1.07	0.31	1.38

compressed cube (**1**) (Scheme 2, right, Table 1, row 3) reduces the pre-edge intensity, i.e., the Fe−S bond covalency, by 0.21 units (sulfides and thiolates). However, elongation of the H-bonded cube allows the electronic structure to adjust to compensate for the loss in bonding which reduces the overall loss of Fe−S covalency to 0.13 units, close to the rescaled experimental value of 0.11 units.[32] This indicates that both elongation and H-bonding comparably contribute to the experimentally observed decrease in covalency of **2** relative to **1**.

An interesting feature of the calculations is that they indicate that the spin topologies of the compressed (**1**) and elongated (**2**) clusters are different. A compressed $[Fe_4S_4]^{2+}$ cube favors a vertical spin topology (Scheme 3, left), where the C_2 axis passes through the two delocalized $S = 9/2$ $[Fe_2S_2]^+$ subclusters antiferromagnetically coupled to each other. The alternate horizontal topology (Scheme 3, right), where the C_2 axis is oriented along these subclusters, is higher in energy by 2.5 kcal/mol. This is because the four shorter Fe−S bonds (2.25 Å, in black, Scheme 3 left) along the C_2 axis of the compressed cluster favor antiferromagnetic coupling between the two Fe_2S_2 clusters (marked in blue and red) bridged by these bonds. Alternatively, the eight Fe−S bonds within the two Fe_2S_2 subclusters are longer, resulting in weaker antiferromagnetic exchange, hence favoring delocalization in these Fe_2S_2 subclusters. However, in the H-bonded cluster (**2**), the horizontal spin topology is found

Scheme 3. Spin Topology of a Compressed (**1**) (Vertical) and an Elongated (**2**) (Horizontal) $[Fe_4S_4]^{2+}$ Cluster

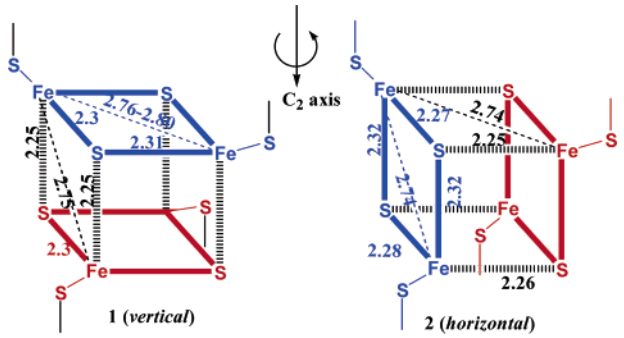

to be more stable by 2.5 kcal/mol. This is because the Fe−S bonds along the C_2 axis are longer in **2** (2.32 Å, Scheme 3 right) and, hence, favor delocalization in the set of the Fe_2S_2 subclusters containing these bonds (in blue and red). The four shorter Fe−S bonds (2.25 Å, in black, Scheme 3 right) are oriented perpendicular to the C_2 axis, which favors antiferromagnetic coupling between these sets of Fe_2S_2 subclusters, stabilizing the horizontal spin orientation in **2**. The calculated wave function for the horizontal spin orientation in **2** shows a change of 0.09 units (Table 1, row 5) of pre-edge intensity in close agreement with the experiment (0.11). Full geometry optimization performed on the simplified (with MeS^-) elongated and contracted clusters also showed that, though the minima of the two optimized structures having vertical and horizontal spin topologies are almost the same, there are quantitatively similar differences

(33) In contrast to the small models with no H-bonding which were fully geometry optimized, the larger H-bonded models were partially optimized (keeping the nitrogen of the H-bonding amide groups frozen in space and optimizing the rest) to maintain the orientation of the H-bonds observed crystallographically.

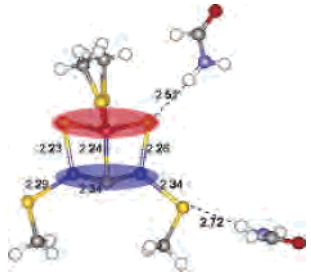

Figure 2. DFT geometry-optimized, H-bonded $[Fe_4S_4]^{2+}$ cube with vertical spin topology.

in energies (about 3 kcal/mol) between the two different spin topologies in any given optimized minima.

The possibility that the elongation observed in this H-bonded cluster (**2**) derives from the H-bonding interactions was explored by geometry-optimized DFT calculations. The calculations show that, when two H-bonding interactions were included in the compressed structure **1** at a slightly longer distance than reported in the structure for **2** and the structure was partially optimized with the H-bond-donor amide groups frozen in space, no structural elongation of the compressed core of **1** was observed (Figure 2).[33] This indicates that the H-bonding energy was not enough to compensate for the core destabilization due to elongation (Figure 2). The optimized structure was distorted due to this H-bonding interaction as evident from asymmetric $Fe-S_{sulfide}$ and $Fe-S_{thiolate}$ bond lengths.[34] The elongation observed in the crystal structure may have contributions from steric interaction with the closely spaced counterion and ether molecules that co-crystallize with **2**.

Discussion

Sulfur K-edge XAS of complexes **1** and **2** show a decrease in pre-edge intensity (Figure 1), indicating a decrease in Fe−S bond covalency. DFT calculations on clusters **1** and **2** reproduce the experimental data and further show that the observed decrease in Fe−S bond covalency is associated with both $\mu_3S_{sulfide}$ and $S_{thiolate}$ and has contributions from both the H-bonding interactions and elongation of the $[Fe_4S_4]^{2+}$ cube in **2**. Since our past results have shown that the redox potentials of Fe_4S_4 cubes decrease linearly with the experimentally observed decrease in Fe−S bond covalency,[13,35] this study indicates that cluster distortions, as well as H-bonding, as observed in **2**, may increase redox potentials of Fe_4S_4 clusters through a decrease in covalency.

DFT calculations on the compressed (**1**) and elongated (**2**) $[Fe_4S_4]^{2+}$ cubes (Scheme 3) indicate that the different clusters favor different spin topologies. A vertical spin topology was favored in the compressed cluster which is generally observed, while the elongated cluster (i.e., **2**) prefers the horizontal topology. This difference in spin topology originates from the fact that shorter Fe−S bonds provide stronger superexchange pathways and favor antiferromagnetism, while longer Fe−S bonds have weaker superexchange couplings, allowing the *double exchange* interactions to dominate, which stabilizes the ferromagnetic ground state in an $[Fe_2S_2]^+$ subcluster. Note that, in a $[Fe_4S_4]^{2+}$ cube, oxidation or reduction occurs within these delocalized $[Fe_2S_2]^+$ subclusters.[32,36]

The $[Fe_4S_4]^{2+}$ cubes in protein active sites of HiPIPs and bacterial ferredoxins are generally compressed. Thus, the magneto-structural correlation developed above can be used to identify the orientation of these redox-active delocalized subunits in an enzyme active site wherever high-resolution crystal structures are available. A distinct axis of compression is observed in a high-resolution crystal structure of the HiPIP from *Chromatuim vinosum*.[37] On the basis of the above correlation, a vertical orientation of the two delocalized $[Fe_2S_2]^+$ subclusters should be stable (Figure 3a, highlighted in blue and red). This orientation suggests that the residues Cys63 and Cys77 are coordinated to one delocalized $[Fe_2S_2]^+$ subcluster, while Cys46 and Cys43 are coordinated to the other delocalized subcluster. The same coordination mode has been suggested (the pair-of-pairs model) via pairwise assignment of β-CH_2 protons of the coordinated cysteines from 2D NMR experiments on the oxidized HiPIP proteins[38] by Bertini et al.[39] Likewise, a high-resolution crystal structure of a $2[Fe_4S_4]$ ferredoxin protein from *Clostridium acidurici* shows an axis of compression (black arrow in Figure 3b).[40] 2D NMR experiments on the reduced $[Fe_4S_4]^+$ clusters have specifically identified residues Cys8 and Cys14 coordinated to one Fe_2S_2 subcluster, while Cys47 and Cys11 are ligated to the other subcluster. The magneto-structural correlation developed above suggests the same coordination mode in the resting $[Fe_4S_4]^{2+}$ form (subclusters shaded red, coordinated by Cys14 and Cys8 and subcluster shaded blue, coordinated by Cys47 and Cys11, in Figure 3b).[41]

The above correlations suggest that the orientation of the delocalized $[Fe_2S_2]^+$ subclusters for both HiPIP and ferredoxins remains the same in all redox states, indicating that the oxidation or reduction process is primarily *localized* in one of the two $[Fe_2S_2]$ subclusters. In the case of ferredoxins, it is the solvent-exposed $[Fe_2S_2]^+$ subcluster (Figure 3b, blue) that localizes the electron in the reduced state. Reduction of the solvent-exposed subcluster may be thermodynamically more favorable, as hydrogen bonding from the solvent will stabilize the additional charge obtained upon reduction. Also,

(34) Note that, when a compressed cluster is given a horizontal spin topology, the system optimizes to an elongated cluster with horizontal spin topology having the same energy as the original compressed cluster with its vertical spin topology. However, when the H-bonded compressed cube is given a horizontal topology, it optimizes to an elongated cluster with horizontal spin topology 0.2 eV higher in energy than the optimized compressed cluster with its vertical spin topology. Hence, there seems to be no energetic driving force for the H-bonded cube to elongate.

(35) Glaser, T.; Hedman, B.; Hodgson, K. O.; Solomon, E. I. *Acc. Chem. Res* **2000**, *33*, 859−868.
(36) Mouesca, J. M.; Noodleman, L.; Case, D. A.; Lamotte, B. *Inorg. Chem.* **1995**, *34*, 4347−4359.
(37) Parisini, E.; Capozzi, F.; Lubini, P.; Lamzin, V.; Luchinat, C.; Sheldrick, G. M. *Acta Crystallogr. D* **1999**, *55*, 1173−1184.
(38) Note that 1D NOE NMR experiments can identify the β-CH_2 protons of the cysteines coordinated to the $Fe^{2.5+}$ species but cannot identify the spin topology of the cluster, unlike the oxidized form.
(39) Bertini, I.; Ciurli, S.; Dikiy, A.; Luchinat, C. *J. Am. Chem. Soc.* **1993**, *115*, 12020−12028.
(40) Dauter, Z.; Wilson, K. S.; Sieker, L. C.; Meyer, J.; Moulis, J. M. *Biochemistry* **1997**, *36*, 16065−16073.
(41) Bertini, I.; Capozzi, F.; Luchinat, C.; Piccioli, M.; Vila, A. J. *J. Am. Chem. Soc.* **1994**, *116*, 651−660.

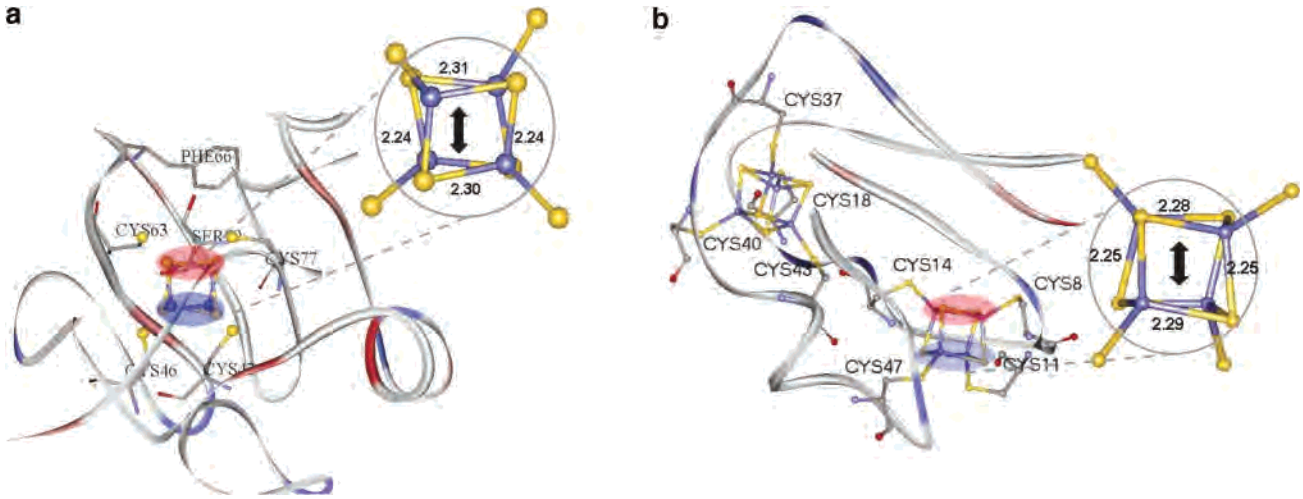

Figure 3. Ribbon diagrams of HiPIP (pdb code 1CKU at 0.9 Å resolution) and ferredoxin (pdb code 1FDN at 1.8 Å resolution) protein showing the orientation of the delocalized $[Fe_2S_2]^+$ clusters of the $[Fe_4S_4]^{2+}$ cube. The axis of core compression is indicated with a black arrow.

the solvent-exposed, redox-active $[Fe_2S_2]^+$ subcluster provides such direct interaction which correlates well with the proposal that in ferredoxin the redox active molecular orbital (RAMO) is mainly Fe based, and hence, it needs direct electron transfer with its partner.

Acknowledgment. This research was supported by NSF Grant No. CHE-0446304 (E.I.S.), NIH Grant No. RR-01209 (K.O.H.), and by NSF Grant No. CHE-0316608 (M.A.W.). Stanford Synchrotron Radiation Laboratory operations are funded by the Department of Energy, Office of Basic Energy Sciences. The SSRL Structural Molecular Biology Program is supported by the National Institutes of Health, National Center for Research Resources, Biomedical Technology Program, and by the Department of Energy, Office of Biological and Environmental Research.

Supporting Information Available: The coordinates of the clusters used for calculation (both simplified and optimized) and a sample input file for the broken symmetry calculation. This material is available free of charge via the Internet at http://pubs.acs.org.

IC050981M